

## Evaluating the particle densities of subarctic soils using pedotransfer functions and vis–NIR spectroscopy

Weber, Peter L.; Hermansen, Cecilie; Norgaard, Trine; Pesch, Charles; Møldrup, Per; Greve, Mogens Humlekrog; Arthur, Emmanuel; de Jonge, Lis Wollesen

*Published in:*  
Soil Science Society of America Journal

*DOI (link to publication from Publisher):*  
[10.1002/saj2.20410](https://doi.org/10.1002/saj2.20410)

*Creative Commons License*  
CC BY 4.0

*Publication date:*  
2022

*Document Version*  
Publisher's PDF, also known as Version of record

[Link to publication from Aalborg University](#)

*Citation for published version (APA):*  
Weber, P. L., Hermansen, C., Norgaard, T., Pesch, C., Møldrup, P., Greve, M. H., Arthur, E., & de Jonge, L. W. (2022). Evaluating the particle densities of subarctic soils using pedotransfer functions and vis–NIR spectroscopy. *Soil Science Society of America Journal*, 86(4), 964-978. <https://doi.org/10.1002/saj2.20410>

### General rights

Copyright and moral rights for the publications made accessible in the public portal are retained by the authors and/or other copyright owners and it is a condition of accessing publications that users recognise and abide by the legal requirements associated with these rights.

- Users may download and print one copy of any publication from the public portal for the purpose of private study or research.
- You may not further distribute the material or use it for any profit-making activity or commercial gain
- You may freely distribute the URL identifying the publication in the public portal -

### Take down policy

If you believe that this document breaches copyright please contact us at [vbn@aub.aau.dk](mailto:vbn@aub.aau.dk) providing details, and we will remove access to the work immediately and investigate your claim.



# ASA, CSSA, and SSSA Virtual Issue Call for Papers: Advancing Resilient Agricultural Systems: Adapting to and Mitigating Climate Change

Content will focus on resilience to climate change in agricultural systems, exploring the latest research investigating strategies to adapt to and mitigate climate change. Innovation and imagination backed by good science, as well as diverse voices and perspectives are encouraged. Where are we now and how can we address those challenges? Abstracts must reflect original research, reviews and analyses, datasets, or issues and perspectives related to objectives in the topics below. Authors are expected to review papers in their subject area that are submitted to this virtual issue.

## Topic Areas

- Emissions and Sequestration
  - » Strategies for reducing greenhouse gas emissions, sequestering carbon
- Water Management
  - » Evaporation, transpiration, and surface energy balance
- Cropping Systems Modeling
  - » Prediction of climate change impacts
  - » Physiological changes
- Soil Sustainability
  - » Threats to soil sustainability (salinization, contamination, degradation, etc.)
  - » Strategies for preventing erosion
- Strategies for Water and Nutrient Management
  - » Improved cropping systems
- Plant and Animal Stress
  - » Protecting germplasm and crop wild relatives
  - » Breeding for climate adaptations
  - » Increasing resilience
- Waste Management
  - » Reducing or repurposing waste
- Other
  - » Agroforestry
  - » Perennial crops
  - » Specialty crops
  - » Wetlands and forest soils



## Deadlines

Abstract/Proposal Deadline: Ongoing  
Submission deadline: 31 Dec. 2022






## How to submit

Submit your proposal to  
[manuscripts@sciencesocieties.org](mailto:manuscripts@sciencesocieties.org)

Please contact Jerry Hatfield at  
[jerryhatfield67@gmail.com](mailto:jerryhatfield67@gmail.com) with any questions.



# Evaluating the particle densities of subarctic soils using pedotransfer functions and vis–NIR spectroscopy

Peter Lystbæk Weber<sup>1</sup>  | Cecilie Hermansen<sup>1</sup>  | Trine Nørgaard<sup>1</sup>  |  
Charles Pesch<sup>2</sup>  | Per Moldrup<sup>2</sup> | Mogens H. Greve<sup>1</sup> | Emmanuel Arthur<sup>1</sup>  |  
Lis de Jonge<sup>1</sup>

<sup>1</sup>Dep. of Agroecology, Faculty of Technical Sciences, Aarhus Univ., Blichers Allé 20, Tjele DK-8830, Denmark

<sup>2</sup>Dep. of the Built Environment, Faculty of Engineering and Science, Aalborg Univ., Thomas Manns Vej 23, Aalborg Ø DK-9220, Denmark

## Correspondence

Peter L. Weber, Dep. of Agroecology, Faculty of Technical Sciences, Aarhus Univ., Blichers Allé 20, Tjele, Denmark, DK-8830.  
Email: [plw@agro.au.dk](mailto:plw@agro.au.dk)

Assigned to Associate Editor Aaron Daigh.

## Funding information

Teknologi og Produktion, Det Frie Forskningsråd, Grant/Award Number: 022-00184B

## Abstract

The particle density ( $\rho_s$ ) is a fundamental physical property needed for calculating the soil porosity and phase distributions. While  $\rho_s$  is often estimated using soil organic matter (SOM) content and particle size distribution, the specific densities of each soil component remain unclear in a subarctic agricultural setting. This study aimed to evaluate the  $\rho_s$  of soils from Southwest Greenland using a three-compartment model (3CM) based on the mixing ratio of SOM derived from loss-on-ignition, mineral particles <20  $\mu\text{m}$  (FC), and mineral particles  $\geq 20 \mu\text{m}$  (CC). We further evaluated the accuracy of the 3CM against pedotransfer functions (PTFs) and visible near-infrared (vis–NIR) spectroscopic models. A total of 324 soil samples from 16 Greenlandic agricultural fields were investigated, covering a wide range in SOM content (0.021–0.602  $\text{kg kg}^{-1}$ ) and clay content (0.020–0.185  $\text{kg kg}^{-1}$ ). Despite their high SOM content, the Greenlandic soils exhibited relatively high  $\rho_s$  (1.936–3.044  $\text{Mg m}^{-3}$ ), which together with a large SOM/organic carbon ratio of 2.16 indicated a high SOM density of 1.493  $\text{Mg m}^{-3}$ . The 3CM fit on all soils indicated FC and CC densities of 3.047 and 2.713  $\text{Mg m}^{-3}$ , respectively, while a subset of soils ( $n = 203$ ) from the same geological setting resulted in FC and CC densities of 2.738 and 2.731  $\text{Mg m}^{-3}$ . Prediction accuracy of the 3CM ( $\text{RMSE} = 0.067 \text{ Mg m}^{-3}$ ) was similar to PTFs ( $\text{RMSE} = 0.068\text{--}0.070 \text{ Mg m}^{-3}$ ) and better than vis–NIR spectroscopic models ( $\text{RMSE} = 0.091 \text{ Mg m}^{-3}$ ).

**Abbreviations:** 3CM, three-compartment model; CC, content of coarse silt and sand; CL, clay content; FC, fines content; IG, Igaliku;  $\text{LOI}_{550}$ , loss-on-ignition at 550 °C; OC, organic carbon content; QA, Qassarsuk; RMSE, root mean square error; SI, South Igaliku; SMS, soil mineral substance; SOM, soil organic matter; SWL, structural water loss; UP, Upernavarsuk; vis–NIR, visible near-infrared;  $\rho_s$ , particle density.

This is an open access article under the terms of the [Creative Commons Attribution](https://creativecommons.org/licenses/by/4.0/) License, which permits use, distribution and reproduction in any medium, provided the original work is properly cited.

© 2022 The Authors. Soil Science Society of America Journal © 2022 Soil Science Society of America.



# 1 | INTRODUCTION

Climate change disproportionally affects the Arctic regions, which are warming at two to three times the global average rate (Serreze & Barry, 2011; Smith et al., 2019). While the rapid warming has profound environmental and socioeconomic ramifications (Nuttall, 2018), the warming climate also prolongs the growing season in Southwest Greenland (Christensen et al., 2016; Westergaard-Nielsen et al., 2015). The shift in climatic conditions also imposes a need to adapt the existing farming activity, which dates back more than a millennium in Southwest Greenland (Dugmore et al., 2007). Little is known about the present and future state of the subarctic agricultural soils in Southwest Greenland, but knowledge of the most fundamental soil properties is needed to support the agricultural activities on these highly organic soils (Caviezel et al., 2017).

The soil particle density ( $\rho_s$ ) is a fundamental physical property, which is defined as the mass per unit of volume for the solid particles. Knowledge of the  $\rho_s$  is needed for determining volumetric phase distributions, which in turn is used for evaluating, for example, the mechanical and thermal properties of soil (Ochsner et al., 2001; Soane, 1990), as well as the diffusive and convective transport of liquids and gases (Deepagoda et al., 2011; Moldrup et al., 2000; Šimůnek et al., 2008). However, due to the laborious and time-consuming measurement procedure,  $\rho_s$  is often not measured during routine soil inventories (McBride et al., 2011). Consequently, the  $\rho_s$  has often been ascribed the value of quartz ( $2.65 \text{ Mg m}^{-3}$ ), which may result in significant errors due to  $\rho_s$  varying considerably across soil types, geography, and even within the same field (Ball et al., 2000; Weber et al., 2020).

A range of compartment models have successfully been developed to predict the  $\rho_s$  from the mass proportions of soil organic matter (SOM) and the mineral matrix (Adams, 1973; McBride et al., 2012; Rühlmann et al., 2006), and recent studies have further expanded on these compartment models to include effects of the particle size distribution (Rühlmann, 2020; Schjønning et al., 2017), mineral composition (Rühlmann & Körschens, 2020), and even SOM quality (Rühlmann, 2020). Despite being presented in multiple forms and various degrees of complexity, the majority of compartment models for  $\rho_s$  can be reduced to a weighted mean of the particle densities for each soil component following McBride et al. (2012):

$$\frac{1}{\rho_s} = \sum_{i=1}^n \left( \frac{m_i}{\rho_i} \right) \quad (1)$$

where  $\rho_s$  is the average particle density of the soil ( $\text{Mg m}^{-3}$ ),  $m_i$  is the mass proportion of the  $i$ th soil component ( $\text{kg kg}^{-1}$ ), and  $\rho_i$  is the density of the soil component ( $\text{Mg m}^{-3}$ ).

## Core Ideas

- The particle density of South Greenlandic soils ranged from  $1.94$  to  $3.04 \text{ Mg m}^{-3}$ .
- Soil organic matter and soil fines content ( $<20 \mu\text{m}$ ) were primary drivers of particle density.
- A three-compartment model was developed for particle density from soil organic matter, fines content, and soils particles  $>20 \mu\text{m}$ .
- The three-compartment model accuracy was similar ( $\text{RMSE} = 0.068 \text{ Mg m}^{-3}$ ) to pedotransfer functions and better than spectroscopic models.
- Organic C-based compartment models require careful consideration of the soil organic matter/organic C content ratio.

The main advantage of compartment models is that they provide density estimates for each soil component if the mass proportions are accurately partitioned. Quantifying the SOM, and thereby accurately partitioning the mineral and organic components, is not straightforward because SOM estimations based on loss-on-ignition (LOI) are affected by structural water loss (SWL) from the mineral matrix during ignition (Jensen et al., 2018; Sun et al., 2009). Moreover, estimations of SOM based on organic carbon content (OC) depend on the SOM/OC conversion factor, which may vary considerably as a result of SOM composition (Pribyl, 2010). While the original compartment model by Adams (1973) was based on a LOI approach, recent work has predominantly used the latter approach by estimating the SOM content based on standardized or theoretical conversion factors (Manage et al., 2019; Rühlmann, 2020; Rühlmann & Körschens, 2020; Schjønning et al., 2017). The application of unsupervised conversion factors may ultimately result in erroneous particle densities of the modelled subcomponents. For instance, using a SOM/OC conversion factor that is too low will result in underestimating the gravimetric SOM content, which will worsen the change in  $\rho_s$  per percentage SOM and thus reduce the perceived density of the SOM fraction. Weber et al. (2020) recently reported a SOM density of  $1.41 \text{ Mg m}^{-3}$  for 170 Greenlandic soils when using a conversion factor of 1.724, which is at the high end of the typical range of  $1.0$ – $1.5 \text{ Mg m}^{-3}$  reported in the literature (Redding & Devito, 2006). However, a later study by Weber et al. (2021) reported a SOM/OC conversion factor of 2.17 for 145 Greenlandic soils from the same area, which indicates that the actual SOM density may have been severely underestimated. The application of unsupervised conversion factors can be disadvantageous, especially for poorly described soils such as the subarctic Greenlandic agricultural soils. It should be noted that  $\rho_s$  models based on OC instead of SOM

circumvents the use of conversion factors entirely, however, such models cannot provide density estimates of individual soil components. Another method, which can be used to predict the  $\rho_s$  is visible-near-infrared spectroscopy (vis-NIRS). This method is a fast and cheap alternative to classical pedo-transfer functions, as a single vis-NIR spectrum can be used to predict numerous soil properties simultaneously (Ben-Dor & Banin, 1995; Chang et al., 2001; Stenberg et al., 2010). The ability to use vis-NIR to predict a wide range of soil properties can be attributed to direct spectral responses from soil moisture, clay minerals, SOM quality and quantity, and electronic transitions of iron oxides (hydration water, hygroscopic water, and/or free water) (Ben-Dor, 2002). Thus, predictions of soil properties that are not spectrally active rely on inter-correlations to spectrally active soil properties. The vis-NIRS has successfully been used to predict both SOM (Kuang & Mouazen, 2011; Viscarra Rossel & Behrens, 2010) and texture (Hermansen et al., 2017; Islam et al., 2003). These are soil properties with direct spectral signatures, but vis-NIRS was also successfully used to predict the  $\rho_s$  of 179 Danish and German soils by Manage et al. (2019), who concluded that the prediction of  $\rho_s$  was favorable for soils exhibiting a large range in SOM contents (0.002–0.67 kg kg<sup>-1</sup>). Further, vis-NIR has been used to predict  $\rho_s$  of 220 soils from Kurdistan, for which the OC ranged from 0.003 to 0.091 kg kg<sup>-1</sup> and the predominant soil textural classes were clay, clay loam, and silt loam (Davari et al., 2021). The  $\rho_s$  was predicted with acceptable accuracy (RMSE of 0.05 Mg m<sup>-3</sup>) in the study of Davari et al. (2021), and the ability to predict  $\rho_s$  from vis-NIR spectra was attributed to spectral responses from clay.

Despite the availability of compartment models, their applicability for cultivated subarctic soils has not been evaluated yet with supervised conversion factors. Thus, the primary aim of this study was to evaluate the  $\rho_s$  of a wide range of subarctic agricultural soils from Southwest Greenland using LOI-based compartment models, which include the effects of structural water loss on SOM determination. The secondary aim of the study was to compare the predictive power of the compartment models to the best performing vis-NIR models and simple linear PTFs.

We hypothesize that these subarctic soils will exhibit a relatively high SOM density compared with the typical range reported in the literature and that vis-NIR spectroscopy can be used as a rapid and cost-effective alternative due to the extensive range in SOM of the Greenlandic soils.

## 2 | MATERIALS AND METHODS

### 2.1 | Study sites

The study included 324 soil samples originating from 16 pasture and cultivated fields dispersed across the Igalikup Kangerlua and Tunulliarfik fjord systems in Southwest Green-

land (Figure 1b), which lies in the marginal ice-free border between the Labrador Sea and the Greenland ice sheet (Figure 1a).

This mountainous agricultural landscape has been designated a UNESCO world heritage site due to its rich agricultural history that dates back to the Norse Landnám about 985 AD. As seen in Figure 1b, the investigated fields are clustered around four agricultural areas of Qassiarsuk (QA, 61°09' N 45°30' W), Igaliku (IG, 61°00' N, 45°26' W), Sdr. Igaliku (SI, 60°53' N, 45°16' W), and Upernaviarsuk (UP, 60°44'57.3" N, 45°53'24.4" W).

The study area is situated within the Palaeoproterozoic Ketilidian Julianehåb batholith (ca. 1800 Ma), an igneous complex dominated by granitic and granodioritic rocks (Garde et al., 2002). The geology is, however, much more complicated in the QA area, where rift magmatism in the Mesoproterozoic resulted in the sandstone and basalt dominated Eriksfjord Formation (Upton, 2013; Upton et al., 2003) being interlayered with lavas, pyroclastic rocks, and intrusions of alkaline silicate rocks and carbonatites (Andersen, 2008). Overall, the investigated fields can be roughly separated into glaciofluvial deposits of granitic origin (IG and UP), Aeolian deposits of granitic origin (SI), and soils of complex volcano-sedimentary origin (QA).

The study area is located to the South of the discontinuous permafrost zone (Daanen et al., 2011), and the climate is subarctic as the mean temperature in July is 10.3 °C in the inner parts of the fjords. Depending on the proximity to the ocean, the mean annual temperature and precipitation range between 0.6 and 0.9 °C and 615 and 858 mm, respectively (Hanna & Cappelen, 2002), and the mean number of growing days ( $\geq 5$  °C) is approximately 146 in the inner part of the fjords (Caviezel et al., 2017).

The vegetation of the fields consisted of perennial grass mixtures including, inter alia, colonial bentgrass (*Agrostis tenuis* L.), Kentucky bluegrass (*Poa pratensis* L.), perennial ryegrass (*Lolium perenne* L.), red fescue (*Festuca rubra* L.), timothy (*Phleum pratense* L.), and wild unsown grass species.

### 2.2 | Soil sampling and analysis

Bulk soil samples of approximately 2 kg were extracted from the upper 5 cm of soil immediately below the turf layer. The depth of the turf layer ranged between 5 and 10 cm, resulting in an effective sampling depth of 5–15 cm. The soil samples were subsequently stored at 2 °C before being air-dried at 20 °C and dry-sieved with a screen size of 2 mm. The OC content was measured directly by high-temperature dry combustion using an ELTRA Helios C-Analyzer (ELTRA GmbH), as all soils tested negative for carbonates using a 10% HCl aqueous solution. Soil texture was measured by a combination of wet-sieving and the pipette method after the removal of the SOM (Gee & Or, 2002), and the  $\rho_s$  was

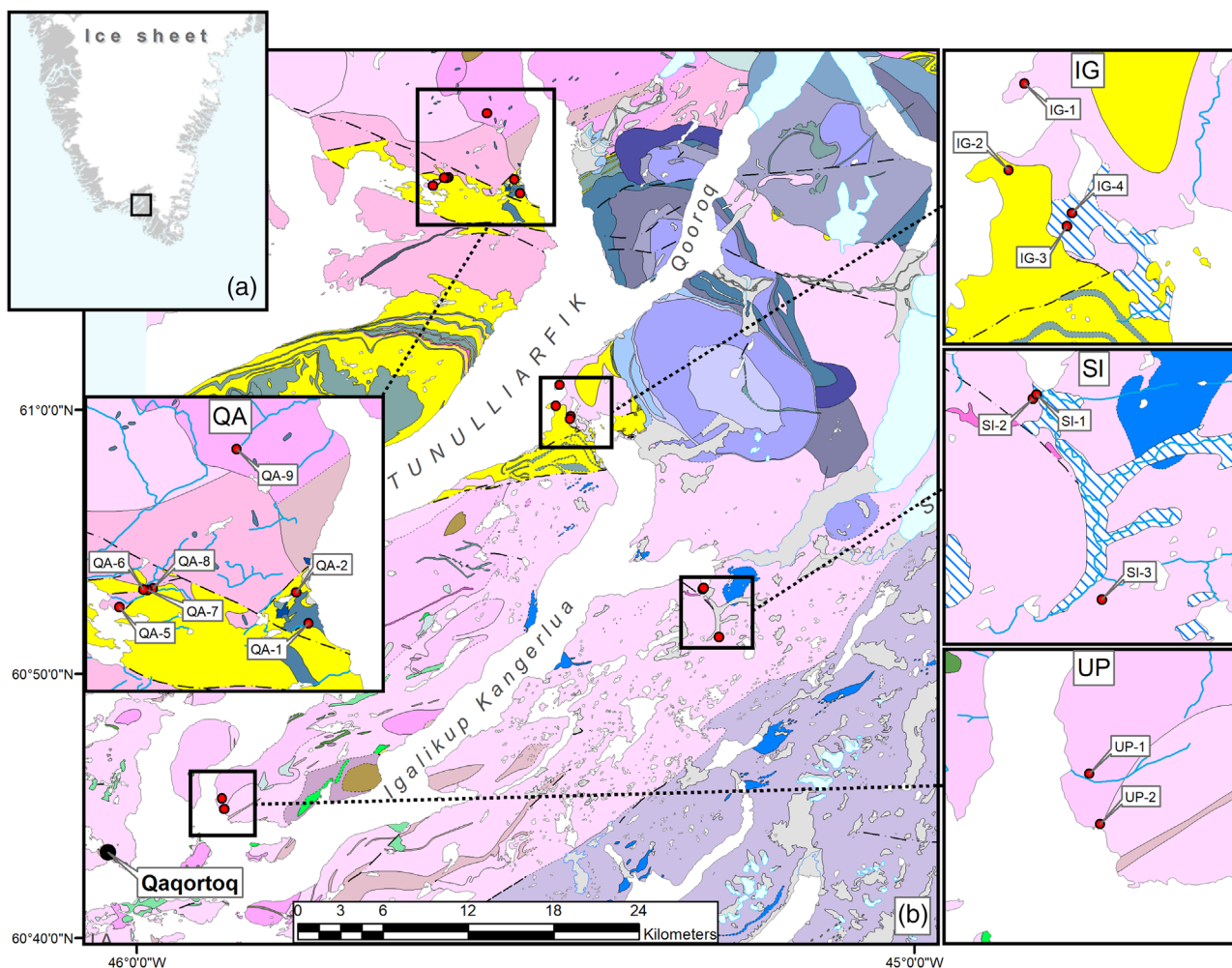


**FIGURE 1** (a) Map showing the broader location of the study area in Southwest Greenland. (b) Geological map showing the geological setting and individual field locations within the four regions Qassarsuk (QA), Igaliku (IG) South Igaliku (SI), and Upernavarsuk (UP). Pink hues denote granitic rocks associated with the Julianehåb batholith, yellow denotes sandstone, and blue-green hues in QA denote a mix of basaltic intrusives, carbonatite, and ultramafic rocks. White/blue stripes denote undifferentiated moraine. GIS map from Kokfelt et al. (2019)

determined in duplicate using the water pycnometer method (Blake & Hartge, 1986). Briefly, 20 g of oven-dry soil (110 °C for 24 h) was mixed thoroughly with 20 °C demineralized water in a 150-ml pycnometer. To ensure the removal of entrapped air, the pycnometer was slowly heated on a hot plate until the sample had boiled for 5 min. The pycnometer was subsequently cooled to 20 °C and subjected to a partial vacuum of approximately 100 mm Hg in a desiccator for 1 h. Loss-on-ignition was determined by oven-drying 6 g of air-dry soil for 24 h at 105 °C and subsequently igniting the samples at 550 °C for 12 h in a half-full Nabertherm L 40/11 muffle furnace (Nabertherm GmbH). The loss-on-ignition at 550 °C (LOI<sub>550</sub>) was reported as the mass loss per unit of oven-dry soil (Hoogsteen et al., 2015).

To circumvent the potential biases of using a fixed SOM/OC conversion factor, we calculated the SOM as

$$\text{SOM} = \text{LOI}_{550} - \text{SWL} \quad (2)$$

where SOM is the soil organic matter ( $\text{kg kg}^{-1}$ ), LOI<sub>550</sub> is the loss-on-ignition at 550 °C ( $\text{kg kg}^{-1}$ ), and SWL is the structural water loss from the mineral matrix during ignition ( $\text{kg kg}^{-1}$ ).

Briefly, the SWL was estimated by approximating the mineral modal abundances, that is, the mass fraction, in each particle size class based on the semi-quantitative mineralogical composition reported for adjacent fields in QA and IG by Rutherford (1995). When the mineral modal abundances are known, the SWL associated with each particle size class can be calculated as:

$$\text{SWL}_{\text{Fraction}} = m_{\text{Fraction}} \times \sum_n \text{SWL}_{\text{Mineral}} \times m_{\text{Mineral}} \quad (3)$$

where  $\text{SWL}_{\text{Fraction}}$  is the SWL associated with each particle size class,  $m_{\text{Fraction}}$  is gravimetric content of the particle size class,  $\text{SWL}_{\text{Mineral}}$  is the SWL associated with each mineral type, and  $m_{\text{Mineral}}$  is the gravimetric content of each mineral



in each particle size class. The  $SWL_{\text{Mineral}}$  were set equal to the values reported by Sun et al. (2009) (Supplemental Table S1).

### 2.3 | Derivation of the three-compartment model

As seen in Equation 1, the specific volume ( $\rho_s^{-1}$ ;  $\text{m}^3 \text{Mg}^{-1}$ ) increases linearly with the volume occupied by all soil components in the mix, which results in a curvilinear relationship of these mixing models with respect to  $\rho_s$ .

Partitioning the soil into a mineral and organic compartment can be achieved by:

$$\text{SMS} = 1 - \text{SOM} \quad (4)$$

where SMS is the total soil mineral substance ( $\text{kg kg}^{-1}$ ). We extended the traditional two-compartment model by further separating the SMS into a mineral fines compartment (FC;  $<20 \mu\text{m}$ ) and coarse silt and sand compartment (CC;  $\geq 20 \mu\text{m}$ ):

$$\text{SMS} = \text{FC} + \text{CC} \quad (5)$$

Rearranging Equation 1 and inserting Equations 4 and 5 yielded a three-compartment (3CM) model:

$$\rho_s = 1 / [(\rho_{\text{SOM}}^{-1} + \text{SOM}) + (\rho_{\text{Fines}}^{-1} \times \text{FC}) + (\rho_{\text{Coarse}}^{-1} \times \text{CC})] \quad (6)$$

where  $\rho_{\text{SOM}}$ ,  $\rho_{\text{Fines}}$ , and  $\rho_{\text{Coarse}}$  are the densities of SOM, FC, and CC compartments, respectively. The  $\rho_{\text{SOM}}$  was derived from a linear fit between the soil specific volume ( $\rho_s^{-1}$ ) and the SOM content, which yields a two-compartment model with SOM and SMS following Equation 1. For this linear function, the  $\rho_{\text{SOM}}^{-1}$  was derived at SOM equal to  $1 \text{ kg kg}^{-1}$ . The 3CM was fitted to the full dataset and a reduced dataset, including only the soils from IG, SI, UP. Further, the  $\rho_{\text{Fines}}$  and  $\rho_{\text{Coarse}}$  were fitting parameters in this function.

### 2.4 | Vis-NIR measurements

Visible-NIR spectra were measured on approximately 50 g air-dry soil using a vis-NIR spectrometer (NIRS DS2500, FOSS) in a climate-controlled laboratory with an average temperature and relative humidity of  $23^\circ\text{C}$  and 48%, respectively. The spectrometer automatically performs seven measurements through the quartz window of a rotating sample cup and reports the average vis-NIR spectra. Lastly, the resulting reflectance spectra were transformed to absorbance:

$$\text{Abs} = \left[ \log \left( \frac{1}{R} \right) \right] \quad (7)$$

where  $R$  is the reflectance at a given wavelength.

### 2.5 | Data analyses and statistics

For qualitative analysis of the measured vis-NIR spectra, the Automatic Weighed Least Squares algorithm was applied for baseline-correction. Further, different spectral preprocessing techniques were tested to optimize model performance. These spectral preprocessing techniques included standard normal variate followed by detrending (Barnes et al., 1989) Savitzky-Golay first and second derivatives (Savitzky & Golay, 1964) as well as gap-segment first and second derivatives (Norris, 2001). The vis-NIR calibration model was made using partial least squares (PLS) regression (SIMPLS algorithm, (de Jong, 1993), and leave-one-out cross-validation was performed to evaluate the model performance. The best combination of spectral preprocessing and calibration model was determined by the root mean square error of the cross-validation ( $\text{RMSE}_{\text{CV}}$ ) and  $r^2$ . The optimal number of factors (NF) was selected where  $\text{RMSE}_{\text{CV}}$  stopped improving significantly (Gowen et al., 2011). The regression coefficients of the resulting calibration models were evaluated to identify the wavelengths of particular importance and subsequently cross-checked with the absorption bands for possible soil components. All multivariate data analysis was performed using the PLS toolbox v. 8.6.2 (Eigenvector Research Inc.) in Matlab.

Pearson's linear correlation coefficient,  $r$ , was used to evaluate the correlation between two parameters, and the goodness of fit was evaluated by the coefficient of determination,  $r^2$ , and adjusted coefficient of determination,  $r^2_{\text{adj}}$ , for linear regressions and multiple linear regressions, respectively. Multiple linear regressions were made with R-project software package v. 4.1.1 (R Core Team, 2021) to create pedo-transfer functions that correlate soil texture and SOM to  $\rho_s$ . Nonlinear optimization of the 3CM was performed with R using the *nls*-function, and model performance was evaluated using the root mean square error.

## 3 | RESULTS AND DISCUSSION

### 3.1 | Soil particle size distribution and organic matter contents

The investigated soils covered a wide range in particle size distributions with a total range in clay, fine silt, and coarse sand of  $0.020\text{--}0.185 \text{ kg kg}^{-1}$ ,  $0.017\text{--}0.239 \text{ kg kg}^{-1}$ , and  $0.015\text{--}0.706 \text{ kg kg}^{-1}$ , respectively (Table 1). Despite



**TABLE 1** Summary of the soil properties for the 234 soils in this study, including soil texture, soil organic matter (SOM), soil organic carbon (OC), particle density ( $\rho_s$ ), and loss-on-ignition at 550 °C (LOI<sub>550</sub>)

Region	Fields	Samples	Statistic	CL	Fsi	Csi	Fsa	Csa	LOI <sub>550</sub>	SOM <sup>a</sup>	OC	$\rho_s$
kg kg <sup>-1</sup>												
Mg m <sup>-3</sup>												
QA	7	121	Mean	0.072	0.110	0.206	0.293	0.156	0.168	0.163	0.077	2.500
			Min.	0.033	0.060	0.064	0.134	0.015	0.046	0.042	0.017	1.936
			Max.	0.168	0.192	0.330	0.426	0.610	0.609	0.602	0.273	3.044
			$\sigma$	0.022	0.021	0.061	0.074	0.118	0.116	0.116	0.054	0.204
IG	4	114	Mean	0.074	0.123	0.191	0.305	0.174	0.142	0.134	0.067	2.469
			Min.	0.027	0.064	0.105	0.135	0.050	0.037	0.021	0.014	2.034
			Max.	0.185	0.239	0.271	0.420	0.412	0.406	0.397	0.195	2.680
			$\sigma$	0.037	0.045	0.041	0.071	0.060	0.065	0.065	0.031	0.112
SI	3	40	Mean	0.030	0.035	0.189	0.474	0.224	0.052	0.048	0.023	2.639
			Min.	0.020	0.017	0.140	0.347	0.133	0.026	0.022	0.009	2.564
			Max.	0.051	0.065	0.252	0.579	0.398	0.096	0.091	0.046	2.699
			$\sigma$	0.008	0.008	0.022	0.059	0.058	0.019	0.018	0.009	0.038
UP	2	49	Mean	0.053	0.092	0.157	0.172	0.414	0.119	0.112	0.057	2.483
			Min.	0.026	0.056	0.073	0.094	0.212	0.036	0.031	0.020	2.283
			Max.	0.085	0.229	0.266	0.334	0.706	0.252	0.242	0.125	2.636
			$\sigma$	0.017	0.040	0.045	0.047	0.093	0.058	0.057	0.027	0.097
All	16	324	Mean	0.065	0.103	0.191	0.301	0.210	0.137	0.131	0.064	2.504
			Min.	0.020	0.017	0.064	0.094	0.015	0.026	0.021	0.009	1.936
			Max.	0.185	0.239	0.330	0.579	0.706	0.609	0.602	0.273	3.044
			$\sigma$	0.030	0.043	0.051	0.104	0.127	0.092	0.091	0.043	0.156

Note. QA, Qassarsuk; IG, Igaliku; SI, South Igaliku; UP, Upernavarsuk; CL, clay (<2  $\mu$ m); Fsi, fine silt (2–20  $\mu$ m); Csi, coarse silt (20–60  $\mu$ m); Fsa, fine sand (60–200  $\mu$ m); Csa, coarse sand (0.2–2 mm);  $\sigma$ , standard deviation. The particle size classes are expressed in kg kg<sup>-1</sup> oven-dry soil, which includes SOM.

<sup>a</sup>The SOM was determined using LOI<sub>550</sub> and subtracting the theoretical structural water loss during ignition (see Supplemental Tables S1 and S2).

the extremely hydrophobic nature of the Greenlandic soils (Weber et al., 2021), the soils did not exhibit issues related to inadequate wetting and floating organic substrate within the pycnometer, which has led some authors to suggest ethanol solutions and nonpolar liquids for organic soils (Blake & Hartge, 1986; Redding & Devito, 2006). While the high-organic soils took slightly longer to saturate, the samples behaved identically approximately halfway through the heating procedure, which indicates that the high-organic soils required more work to saturate. Nevertheless, the replicability was high across all OC contents, with a maximum range between duplicate measurements of 0.012 Mg m<sup>-3</sup>.

The two regions with the highest number of samples, that is, QA and IG, exhibited relatively similar mean values and standard deviations across all particle sizes. Comparatively, the Aeolian sands of SI were dominated by fine sand and contained low amounts of clay and fine silt, while the coarse sand fraction dominated UP soils. The theoretical structural water loss (SWL) associated with the clay and silt fraction was calculated to range between 0.032 and 0.075 kg kg<sup>-1</sup> and 0.003 and 0.007 kg kg<sup>-1</sup>, respectively, and the SWL from the sand fraction was estimated to be 0.002 kg kg<sup>-1</sup> (Supplemental Table S2). The theoretical SWL agreed well with the findings

of Jensen et al. (2018), who reported SWL of clay, silt, and sand of 0.021 kg kg<sup>-1</sup>, 0.005 kg kg<sup>-1</sup>, and 0.0008 kg kg<sup>-1</sup>, respectively, in a Danish agricultural field. Further, Hoogsteen et al. (2015) reported a SWL of 0.075 kg kg<sup>-1</sup> for clay in a set of Dutch clay soils, matching the upper limit for the Greenlandic soils. Nevertheless, SWL had little effect on the calculated SOM values (Supplemental Figures S1 and S2), as the LOI at 550 °C was substantial for these highly organic soils (Figure 1a). Consequently, the SOM ranged between 0.021 kg kg<sup>-1</sup> and 0.602 kg kg<sup>-1</sup> for all soils, with the SI soils having the lowest SOM content with a mean of 0.048 kg kg<sup>-1</sup>.

The obtained SOM contents were strongly linearly correlated ( $r^2 = .97$ ) with the OC content. The linear regression had a small positive intercept, which was insignificant (Figure 2a). The regression slope coefficient was 0.462, which indicates a gravimetric C content in SOM of 46.2% and a SOM/OC conversion factor of 2.16. The obtained regression coefficient from the Greenlandic soils was in the lower end of the range of 0.41–0.73, or SOM/OC of 1.4–2.4, reported by Pribyl (2010). The study of Pribyl (2010) also proposed an upper limit for the SOM/OC conversion factor of 2.5 for young soils with poorly decomposed SOM, consisting predominantly of compounds with low C concentrations, for example,

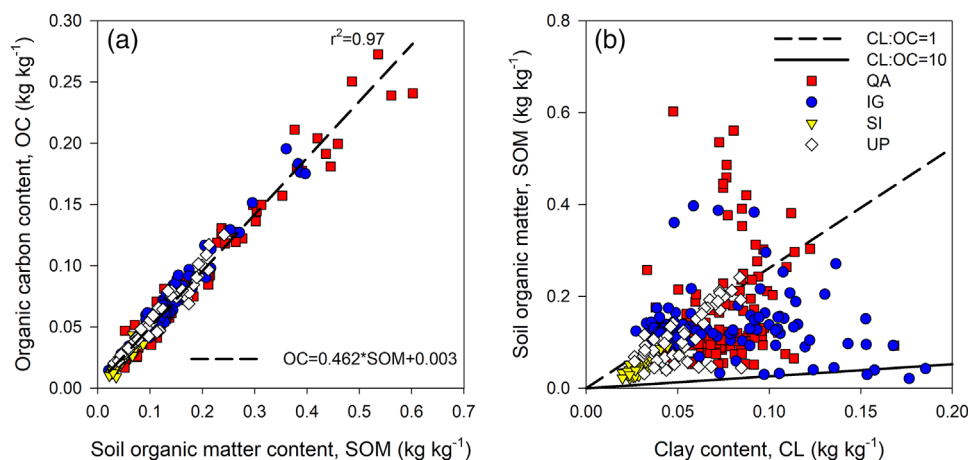


**FIGURE 2** (a) Organic carbon content (OC) as a function of soil organic matter (SOM) for the investigated soils. (b) Soil organic matter as a function of clay (CL) content for the investigated soils with CL/SOM ratios of 1:4.6 (solid) and 1:0.46 (dashed) lines, which corresponds to a CL/OC ratios of 1 and 10, respectively

carbohydrates. The obtained SOM/OC conversion factor of 2.16, although smaller than 2.5, is still significantly larger than the often used factor of 1.724. This may thus reflect a poorly decomposed SOM pool due to the cold climate impeding the microbial decomposition of the SOM. This mechanism is well documented in Cryosols, where poor decomposition of SOM results in carbohydrate-rich and easily decomposable SOM in a particulate form close to the active layer (Ernakovich et al., 2015; Kögel-Knabner & Amelung, 2021; Mueller et al., 2015). Additionally, the investigated soils are highly saturated in SOM, exhibiting CL/OC ratios  $< 10$  (Figure 2b), which indicates a high content of noncomplexed SOM (Dexter et al., 2008) and supports the impression of a poorly decomposed SOM pool. Furthermore, high SOM/OC ratios have previously been reported for subarctic soil. For example, Azevedo et al. (2021) reported a ratio of 2.24 for 23 soils from Abisko in northern Sweden.

### 3.2 | Particle density

The measured  $\rho_s$  ranged from 3.044 to 1.936 Mg m<sup>-3</sup>, with the majority of the samples exhibiting a curvilinear relationship between  $\rho_s$  and SOM when plotted as individual soils (Figure 3a). The QA soils generally exhibited higher and more variable  $\rho_s$  compared with the other regions, especially at low SOM contents, which may be attributed to the varied geological setting in the region. Overall, the Greenlandic soils consistently exhibited higher  $\rho_s$  across the entire SOM range compared with the model developed by Rühlmann et al. (2006) on 163 soils from the United States, India, and northern Europe, which predicted  $\rho_s$  range of 2.608–1.794 Mg m<sup>-3</sup>. The higher  $\rho_s$  of the Greenlandic soils is attributed to a higher density of the SMS ( $\rho_{SMS}$ ) and especially SOM ( $\rho_{SOM}$ ).

The field-average  $\rho_s$  decreased linearly with SOM ( $r^2 = .89$ ) across all the investigated fields (Figure 3b). A

positive correlation ( $r = .33$ ) was evident between FC and  $\rho_s$  for the QA soils (Figure 3d), while no clear correlations were found between FC and both the field average  $\rho_s$  (Figure 3e) and region-wide  $\rho_s$  (Figure 3d) for the IG, IS, and UP soils. An apparent discrepancy was found between the two biggest fields, that is, IG-4 and QA-2, where the  $\rho_s$  of the IG-4 was strongly correlated with SOM ( $r^2 = .98$ ; Figure 3c), and the QA-2 with FC ( $r^2 = .59$ ; Figure 3f).

### 3.3 | Vis-NIR spectra

The raw vis-NIR spectra were affected by both FC and SOM content. This can be seen, that is, as a gradient in absorbance throughout the visible range according to both SOM and FC content (Figure 4a), with the samples having the highest SOM and FC content also exhibiting the highest absorbance.

Soil organic matter as well as minerals containing iron oxides absorb light throughout the visible range (Stenberg et al., 2010). The effects of FC and SOM content on spectra in the near-infrared range were enhanced after the application of a baseline filter (Figure 4b). All soils exhibited a peak around 1,400 nm (OH stretch) and 1,900 nm (OH stretch and HOH bend), which are some of the most characteristic absorptions features of soil moisture throughout the vis-NIR spectral range (Clark et al., 1990; Hunt, 1977; Stenberg et al., 2010; Viscarra Rossel & Behrens, 2010). A shift in this peak location for the 1,400 nm absorption feature can be observed when comparing the two soils exhibiting the highest SOM content (1,450 nm) to the two soil samples exhibiting the highest contents of FC (1,414 nm). The two soil samples containing the highest amounts of SOM (0.536 and 0.277 kg kg<sup>-1</sup>) exhibit a peak in absorbance at 1,729 nm, which is a spectral signature associated with the CH bond in organic matter (Viscarra Rossel & Behrens, 2010). Further, all soils in Figure 4

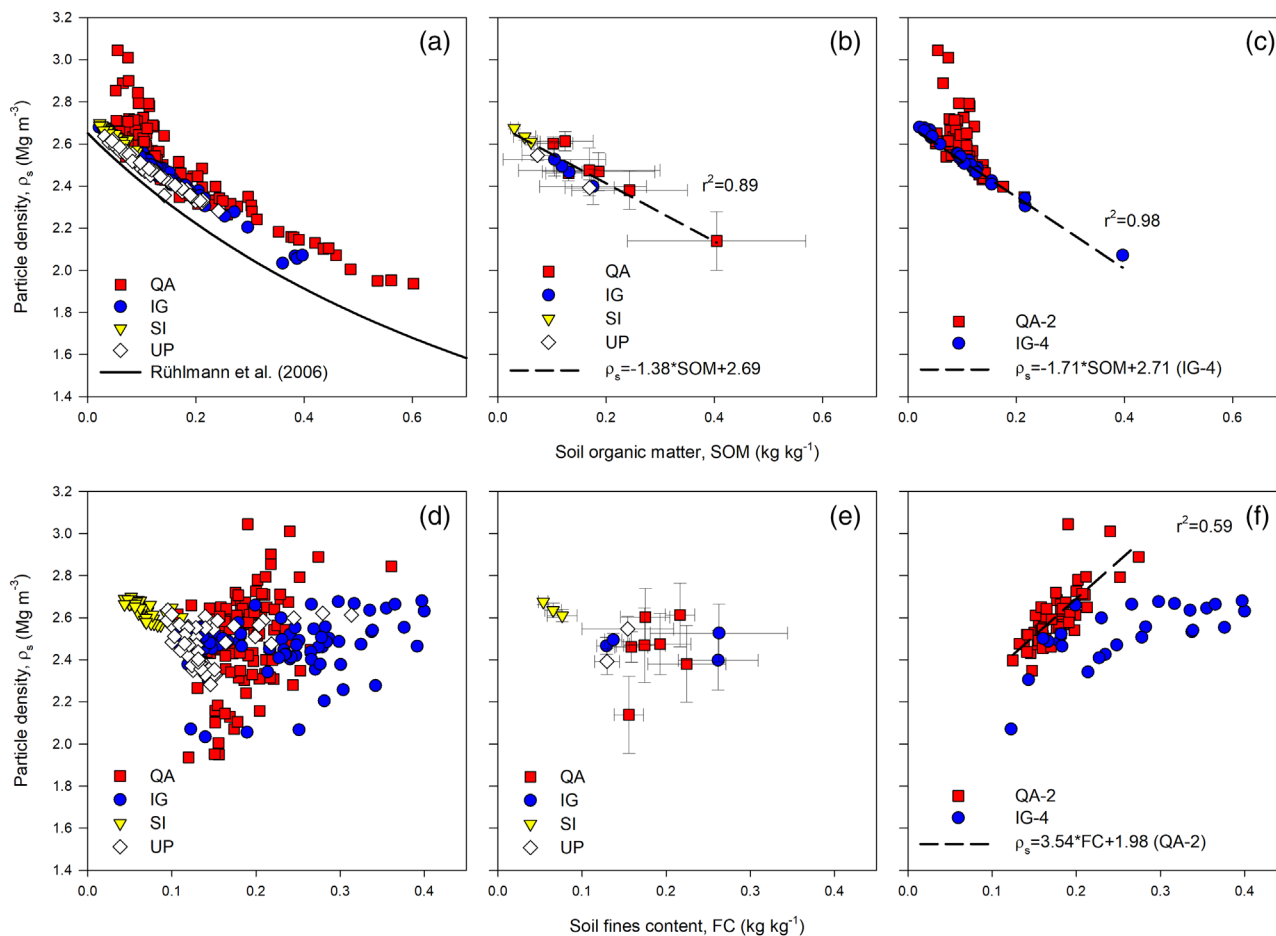


**FIGURE 3** (a) Particle density ( $\rho_s$ ) vs. soil organic matter (SOM), (b) field-average  $\rho_s$  vs. field-average SOM, (c)  $\rho_s$  vs. SOM for a large OM gradient exhibited by field IG-4 (blue circle) and a large gradient in fines content (FC;  $<20 \mu\text{m}$ ) exhibited by field QA-2 (red square), (d)  $\rho_s$  vs. FC for all soil samples, (e) field-average  $\rho_s$  vs. field-average FC, (f)  $\rho_s$  vs. FC for IG-4 and QA-2 with linear regression for QA-2 (dashed). The solid line in “a” represents the relationship between  $\rho_s$  and SOM found by Rühlmann et al. (2006)

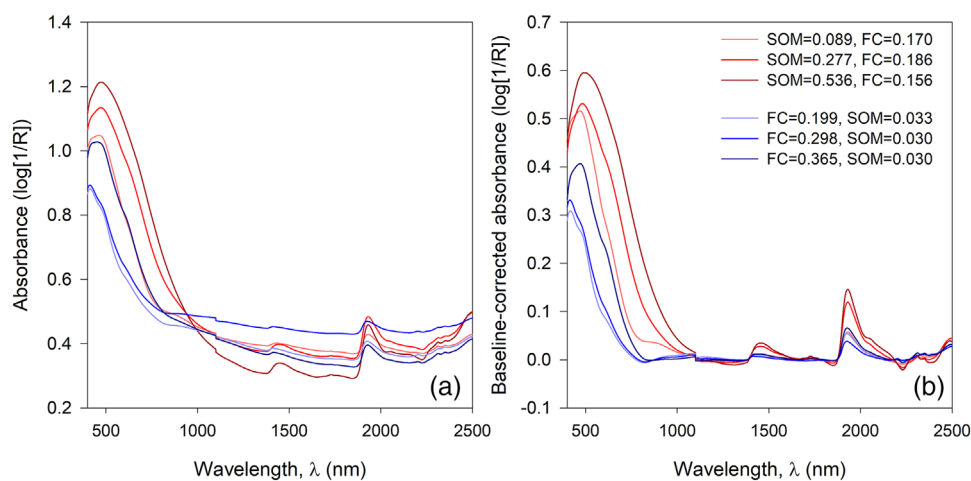


**FIGURE 4** Selected visible near-infrared (vis-NIR) spectra where three represent a soil organic matter (SOM) gradient within field QA-1 from 0.089 to 0.536  $\text{kg kg}^{-1}$  (red gradient), and three representing a gradient in fines content from 0.199 to 0.365  $\text{kg kg}^{-1}$  within field IG-4. The spectra are illustrated as (a) raw spectra and (b) baseline-corrected spectra (algorithm: Automatic Weighted Least Squares)

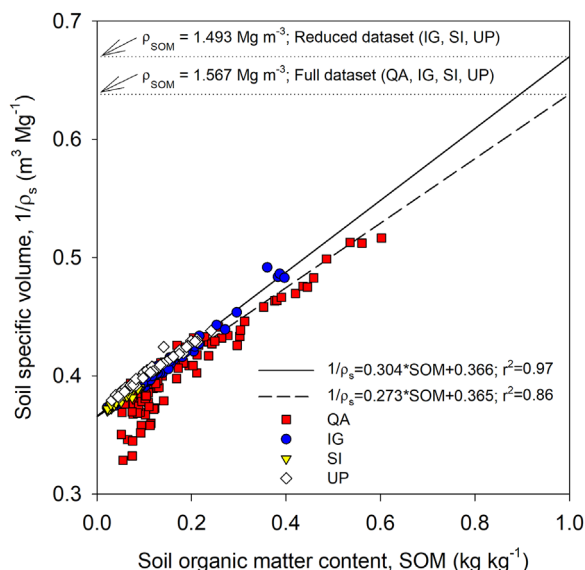


**FIGURE 5** Soil specific volume as a function of soil organic matter content (SOM) with linear regressions for all soils (dashed line) and the reduced dataset (solid line). The linear regressions were extrapolated to  $\text{SOM} = 1 \text{ kg}^{-1}$  to find the specific volume of SOM

exhibited small peaks around 2,310 and 2,350 nm, which may be caused by organic constituents (Stenberg et al., 2010) or absorptions features from Fe/Mg-OH (Fang et al., 2018; Hunt, 1977).

### 3.4 | Three-compartment model

The specific volume ( $1/\rho_s$ ) and SOM exhibited a strongly linear ( $r^2 = .97$ ) relationship for the IG, SI, and UP soils, which indicated a constant  $\rho_s$  of the SOM of  $1.49 \text{ Mg m}^{-3}$  for this reduced dataset (Figure 5). Including the QA soils markedly decreased the  $r^2$  to .86 and resulted in a  $\rho_{\text{SOM}}$  of  $1.57 \text{ Mg m}^{-3}$ , which likely was an artifact due to the variation in mineral densities in the QA soils.

The obtained  $\rho_{\text{SOM}}$  values were higher than the  $1.41 \text{ Mg m}^{-3}$  Weber et al. (2020) reported for 170 Greenlandic soils that were included in the present study. This increase in  $\rho_{\text{SOM}}$  is a direct result of the partitioning of the SOM and SMS fractions, where Weber et al. (2020) used an OC/SOM ratio of 0.58, which is significantly higher than the OC/SOM ratio of 0.462 found in the present study. This highlights the pitfalls of directly comparing or ascribing a physical meaning to the fitting parameters, for example,  $\rho_{\text{SOM}}$  when different and unsupervised conversion factors are used for modeling the OC- $\rho_s$  relationship. Additionally, no evidence was found that the OC/SOM ratio and  $\rho_{\text{SOM}}$  varied across the SOM range, which contrasts the work by Ruehlmann (2020), who hypothesized that both would increase. Nevertheless, the predicted  $\rho_{\text{SOM}}$  was in the high end ( $1.49 \text{ Mg m}^{-3}$ ) or above ( $1.57 \text{ Mg m}^{-3}$ ) the suggested range of  $1.34\text{--}1.52 \text{ Mg m}^{-3}$ , which was

obtained using the LOI-based approach on boreal wetland surface soils (Redding & Devito, 2006), boreal forest soils (Redding et al., 2005), temperate rainforest (Adams, 1973), and pure Finnish sphagnum peat (Heiskanen, 1992).

Due to the divergent behavior of the QA soils, it was decided to use the  $\rho_{\text{SOM}}$  of  $1.49 \text{ Mg m}^{-3}$  to parameterize the 3CM on both the full and reduced datasets. The 3CM resulted in a moderately good fit of the full dataset with an RMSE of  $0.067 \text{ Mg m}^{-3}$  (Figure 6a), and the fitted densities of the FC and CC ( $\rho_{\text{Fines}}$  and  $\rho_{\text{Coarse}}$ ) were  $3.05$  and  $2.71 \text{ Mg m}^{-3}$ , respectively.

Overall, the 1:1 line generally bisected the data resulting in overprediction for the IG and UP soils, while the  $\rho_s$  were underpredicted for the majority of the QA soils. The regional differences in model predictions were likely due to different clay mineralogy and higher  $\rho_{\text{Fines}}$  for the QA soils, which is indicated by the positive correlations between FC and  $\rho_s$  in Figure 3d and 3f. The high  $\rho_{\text{Fines}}$  thus resulted in inflated predictions for the non-QA soils with the largest FC (IG and UP), while the SI soils were well predicted due to their low FC content.

The 3CM excellently fitted the reduced dataset with an RMSE of  $0.019 \text{ Mg m}^{-3}$  (Figure 6b). The fitted  $\rho_{\text{Fines}}$  and  $\rho_{\text{Coarse}}$  were  $2.74$  and  $2.73 \text{ Mg m}^{-3}$ , respectively, which corroborates the discrepancy in  $\rho_{\text{Fines}}$  discussed above. The obtained  $\rho_{\text{Coarse}}$  of  $2.73 \text{ Mg m}^{-3}$  agrees well with the average mineral density of  $2.73 \text{ Mg m}^{-3}$ , which Weber et al. (2020) obtained from a subset of the investigated soils. The fitted  $\rho_{\text{Fines}}$  of  $2.74 \text{ Mg m}^{-3}$  for the reduced dataset is close to the clay densities of  $2.86$  and  $2.761 \text{ Mg m}^{-3}$  reported for large international datasets by Schjønning et al. (2017) and Ruehlmann (2020), respectively. The RMSE of  $0.019 \text{ Mg m}^{-3}$  was low compared with the range of  $0.035\text{--}0.11 \text{ Mg m}^{-3}$ , which was reported in two studies that applied two-compartment models on Canadian soil inventories with a similar range in  $\rho_s$  (McBride et al., 2011; McBride et al., 2012). However, it should be noted that the superior model performance likely results from relatively less confounding factors, for example, soil depth, vegetation, climate, management, soil age, and geological setting, which is relatively homogeneous for the investigated soils when the QA soils are excluded.

### 3.5 | Pedotransfer functions

The simple PTFs using SOM and FC resulted in a decrease in the goodness of fit compared with the three-compartment models (Figure 7). The RMSE for the full dataset increased by  $0.003$  to  $0.070 \text{ Mg m}^{-3}$  with an adjusted  $r^2_{\text{adj}}$  of .80. The effects of both SOM and FC in the regression were statistically significant ( $p < .0001$ ).

The clay-based PTF exhibited similar intercepts and SOM coefficients compared with the FC-based PTFs, but the



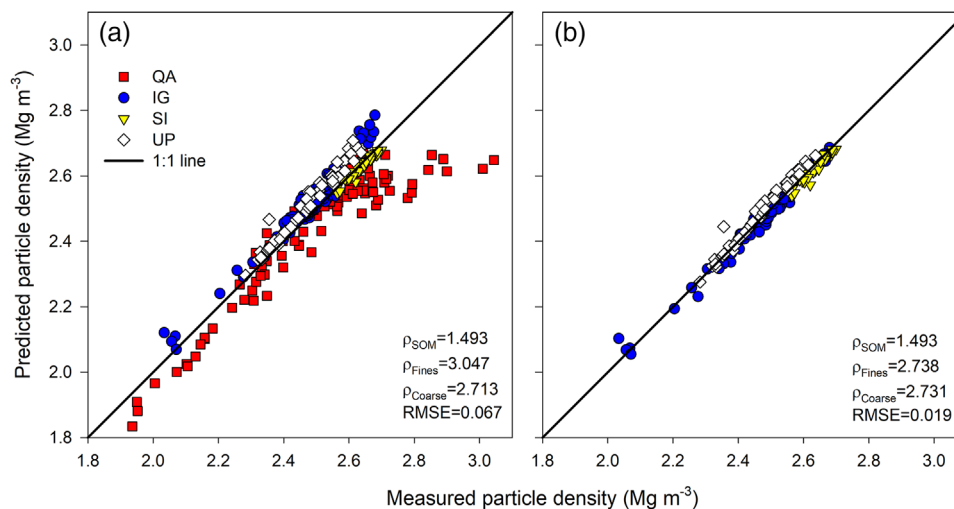


**FIGURE 6** Predicted vs. measured particle densities for the three-compartment model (Equation 6) fitted to (a) the full dataset and (b) the reduced dataset

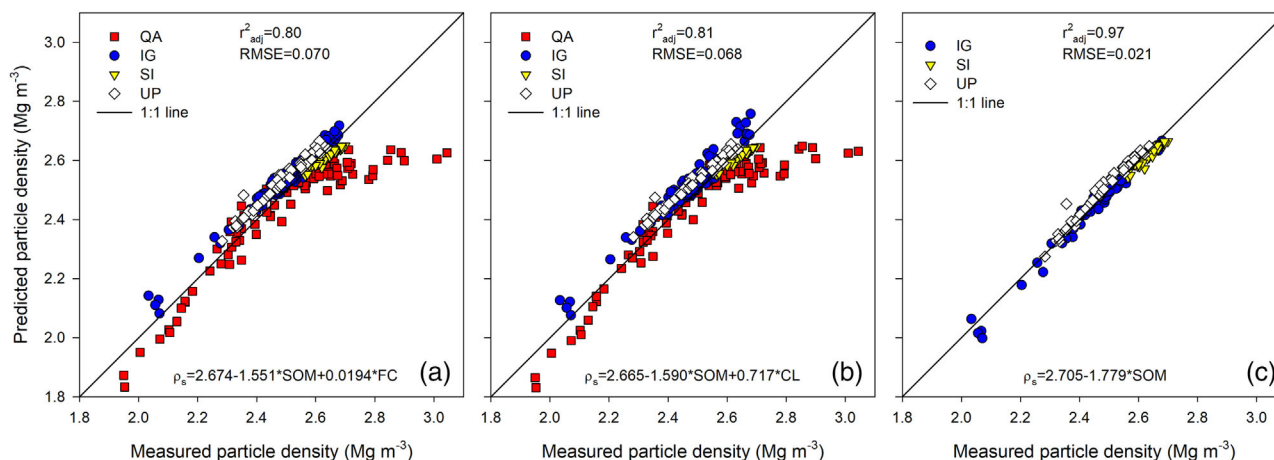


**FIGURE 7** Predicted vs. measured for pedotransfer functions for particle density ( $\rho_s$ ) derived by multiple linear regressions between  $\rho_s$ , soil organic matter (SOM), and either (a) fines content (FC) or (b) clay content (CL) on the full dataset. (c) Best performing pedotransfer function for the reduced dataset

regression coefficients for clay were markedly higher than the regression coefficients obtained for FC (Figure 7b). The overall performance of the clay-based PTFs were slightly higher with an RMSE of 0.068  $\text{Mg m}^{-3}$  and an adjusted  $r^2_{\text{adj}}$  of .81 for the full dataset. The best performing PTF on the reduced dataset was based on only SOM, as the FC and CL did not significantly contribute to  $\rho_s$  (Figure 7b).

### 3.6 | Vis-NIR models

The best performing PLS regression models were obtained using Gap Segment first derivative (segment size: 9 and a gap size: 25) as preprocessing technique. The segment size denotes the number of points across which the spectrum is smoothed, and the gap denotes the gap size in between the

two segments (Norris, 2001). The optimal number of factors was 5 and 8 for the full and reduced dataset, respectively (Figure 8).

The vis-NIR calibration models exhibited a similar trend to the pedotransfer functions, that is, markedly better predictions of  $\rho_s$  when the QA soils were removed from the dataset. The calibration model on the full dataset resulted in an  $\text{RMSE}_{\text{CV}}$  of 0.091  $\text{Mg m}^{-3}$ , and the reduced calibration model resulted in a respectable  $\text{RMSE}_{\text{CV}}$  of 0.030  $\text{Mg m}^{-3}$ , which corresponds to a relative increase compared with the 3CM of 36 and 58%, respectively. The RMSE of the vis-NIR calibration model on the full dataset is comparable with the  $\text{RMSE}_{\text{CV}}$  of 0.10  $\text{Mg m}^{-3}$  obtained in a calibration model for 179 Danish and German topsoils by Manage et al. (2019). Their range in  $\rho_s$  was, however, significantly higher (1.60–2.66  $\text{Mg m}^{-3}$ ), resulting in an  $r^2$  of .87. Manage et al. (2019) posited

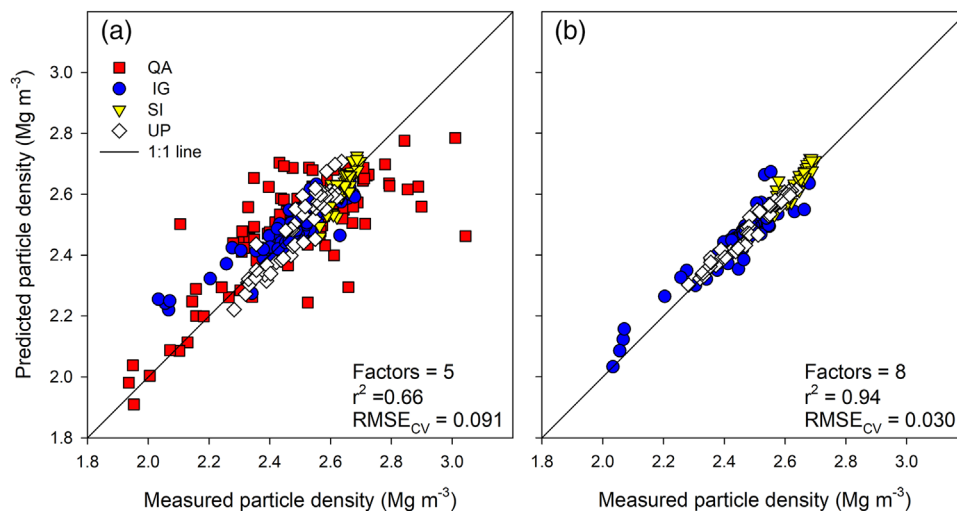


**FIGURE 8** Predicted vs. measured particle densities for the visible near-infrared (vis-NIR) models on (a) the full dataset, and (b) the reduced dataset

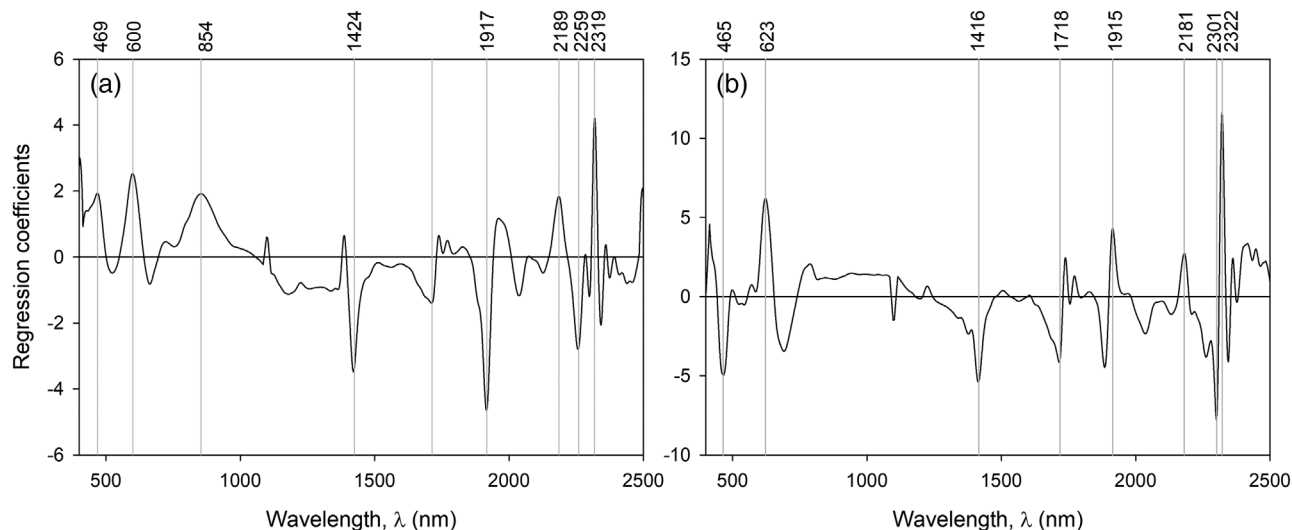


**FIGURE 9** Regression coefficients for visible near-infrared (vis-NIR) models using (a) the full data and (b) the reduced dataset

that the high accuracy obtained in their model was attributed to their extensive range in SOC ( $0.001\text{--}0.451\text{ kg kg}^{-1}$ ), which they supported by only achieving an  $r^2$  of .62 for 83 mineral topsoils with a SOC range of  $0.001\text{--}0.06\text{ kg kg}^{-1}$ . Conversely, clay content was suggested to be the most important chromophore for  $\rho_s$  prediction by Davari et al. (2021), who obtained an  $\text{RMSE}_{\text{CV}}$  of  $0.05\text{ Mg m}^{-3}$  ( $r^2$  of .62) in a calibration model for 220 Kurdistan topsoils with a  $\rho_s$  range of  $2.38\text{--}2.65\text{ Mg m}^{-3}$ . Since the full dataset in the present study exhibits a relatively large OC range ( $0.009\text{--}0.273\text{ kg kg}^{-1}$ ) and a moderate clay range ( $0.020\text{--}0.185\text{ kg kg}^{-1}$ ), the poor performance is likely caused by high variability in the mineralogy and/or the presence of dense sesquioxides of the QA soils, for which the vis-NIR model is unable to account. The vis-NIR calibration model on the reduced dataset resulted in an  $r^2$  of .94, which is markedly higher than the other

efforts reported in the literature. The high accuracy obtained on the reduced dataset is likely due to the soils being from the same geological setting and the lack of confounding factors mentioned in the previous section. The overall performance of the vis-NIR models indicates that vis-NIR spectroscopy may serve as a fast and cost-effective alternative to the traditional approaches of estimating  $\rho_s$ , especially in soils with homogenous parent material.

The regression coefficients from a vis-NIR model can be indicative of which spectral absorption bands are important for predicting a specific independent variable (Haaland & Thomas, 1988). The model on the full dataset (Figure 9a) exhibited peaks around 469 and 600, which is comparable to the model on the reduced dataset (Figure 9b), for which regression coefficient peaks were found at 465 and 623 in the visible range.

These peaks might be related to electronic transitions of iron oxides, for example, hematite (444 and 650 nm) or goethite (480, 488, and 650 nm) (Scheinost et al., 1998). Comparably, the study of Davari et al. (2021) found the wavelengths around 453 and 608 nm to be correlated to  $\rho_s$ . The model on the full dataset exhibit a peak around 854 nm, which could be related to either iron oxides or organic constituents (CH-bond) (Viscarra Rossel & Behrens, 2010; Viscarra Rossel et al., 2006). Both models exhibited peaks due to soil moisture around 1,400 (OH stretch) and 1,900 nm (OH stretch and HOH bend). Several of the regression coefficient peaks are located in spectral regions associated with overtones of the CH stretch (peaks for model on the full dataset: 1,713, 2,259, and 2,319 nm; peaks for model on the reduced dataset: 1,718, 2,301, and 2,322 nm) (Viscarra Rossel & Behrens, 2010). Especially the peak around 2,320 nm is very distinct in both models and could also be related to the combination of Mg-OH bend and OH stretch near 2,300 nm (Viscarra Rossel et al., 2006).

### 3.7 | Model limitations

The  $\rho_s$  models developed herein are based on Greenlandic soils that have a unique pedogenetic process compared with soils in other parts of the world. Consequently, the clay mineralogy is likely to be different from soils from other warmer parts of the world, and the clay contents are quite low ( $<0.20 \text{ kg kg}^{-1}$ ). Furthermore, the organic matter from these fields originate from grass-based materials that are poorly decomposed under subarctic environments. The models are thus optimally applicable to areas that exhibit similar geological properties and soil physical and chemical characteristics.

## 4 | CONCLUSIONS

This study investigated the particle density ( $\rho_s$ ) of soils from the QA, IG, SI, and UP regions, which cover a large part of the agricultural area in Southwest Greenland. A physically based three-compartment model was developed on the mixing ratios SOM, mineral FC ( $<20 \mu\text{m}$ ), and the CC ( $\geq 20 \mu\text{m}$ ), and the model performance was subsequently compared with simple linear pedotransfer functions and vis-NIR spectroscopic models.

The soils exhibited relatively high  $\rho_s$  ranging from 1.936 to  $3.044 \text{ Mg m}^{-3}$ , with the QA region exhibiting a particularly high variation in  $\rho_s$  values due to its complex geological setting. The study showed that SOM and FC were the main controls for these subarctic soils and that the SOM exhibited a high OC/SOM ratio of 2.16. Further, no indication was found that the OC/SOM ratio and the density of SOM varied as a function of SOM content.

All of the three prediction approaches exhibited a significant reduction in model performance when including the QA region, as neither the applied soil data nor the vis-NIR spectra were able to account for the high variability in the mineralogy and/or the presence of dense sesquioxides of these soils. Nevertheless, all three approaches produced adequate results for most uses, especially when used on a dataset with homogeneous parent material.

This study highlights the pitfalls of applying unsupervised SOM conversion factors when ascribing a physical meaning to the fitted densities of the subcomponents, especially when dealing with soil data with a limited range of each subcomponent.

## ACKNOWLEDGMENTS

The authors would like to express their sincere gratitude to the farmers and the Greenlandic Agricultural Consulting Services for their valuable contributions during the fieldwork. Funding: This work was supported by the Danish Council for Independent Research, Technology and Production Sciences via the project: Glacial flour as a new, climate-positive technology for sustainable agriculture in Greenland: NewLand [grant no. 022-00184B].

## AUTHOR CONTRIBUTIONS

Peter Lystbæk Weber: Conceptualization; Data curation; Formal analysis; Investigation; Methodology; Resources; Validation; Visualization; Writing-original draft; Writing-review & editing. Cecilie Hermansen: Conceptualization; Data curation; Formal analysis; Investigation; Methodology; Validation; Visualization; Writing-original draft; Writing-review & editing. Trine Nørgaard: Data curation; Investigation; Methodology; Validation; Writing-review & editing. Charles Marie Henri Emile Pesch: Data curation; Investigation; Validation; Writing-review & editing. Per Møldrup: Conceptualization; Formal analysis; Funding acquisition; Supervision; Writing-review & editing. Mogens Humlekrog Greve: Conceptualization; Funding acquisition; Resources; Supervision; Validation; Writing-review & editing. Emmanuel Arthur: Conceptualization; Data curation; Investigation; Methodology; Supervision; Validation; Writing-review & editing. Lis de Jonge: Conceptualization; Formal analysis; Funding acquisition; Methodology; Project administration; Resources; Supervision; Validation; Writing-review & editing.

## CONFLICT OF INTEREST

The authors declare no conflict of interest.

## ORCID

Peter Lystbæk Weber  <https://orcid.org/0000-0001-9249-0796>

Cecilie Hermansen  <https://orcid.org/0000-0002-1925-3732>

Trine Nørgaard  <https://orcid.org/0000-0001-7669-3841>  
 Charles Pesch  <https://orcid.org/0000-0003-4120-0239>  
 Emmanuel Arthur  <https://orcid.org/0000-0002-0788-0712>

## REFERENCES

- Adams, W. A. (1973). The effect of organic matter on the bulk and true densities of some uncultivated podzolic soils. *Journal of Soil Science*, 24(1), 10–17. <https://doi.org/10.1111/j.1365-2389.1973.tb00737.x>
- Andersen, T. (2008). Coexisting silicate and carbonatitic magmas in the Qassiarsuk complex, Gardar Rift, Southwest Greenland. *The Canadian Mineralogist*, 46(4), 933–950. <https://doi.org/10.3749/canmin.46.4.933>
- Azevedo, O., Parker, T. C., Siewert, M. B., & Subke, J.-A. (2021). Predicting soil respiration from plant productivity (NDVI) in a sub-Arctic tundra ecosystem. *Remote Sensing*, 13(13), 2571. <https://www.mdpi.com/2072-4292/13/13/2571>
- Ball, B. C., Campbell, D. J., & Hunter, E. A. (2000). Soil compactibility in relation to physical and organic properties at 156 sites in UK. *Soil and Tillage Research*, 57(1), 83–91. [https://doi.org/10.1016/S0167-1987\(00\)00145-8](https://doi.org/10.1016/S0167-1987(00)00145-8)
- Barnes, R. J., Dhanoa, M. S., & Lister, S. J. (1989). Standard normal variate transformation and de-trending of near-infrared diffuse reflectance spectra. *Applied Spectroscopy*, 43(5), 772–777. <https://doi.org/10.1366/0003702894202201>
- Ben-Dor, E. (2002). Quantitative remote sensing of soil properties. *Advances in Agronomy*, 75, 173–243. [https://doi.org/10.1016/S0065-2113\(02\)75005-0](https://doi.org/10.1016/S0065-2113(02)75005-0)
- Ben-Dor, E., & Banin, A. (1995). Near-infrared analysis as a rapid method to simultaneously evaluate several soil properties. *Soil Science Society of America Journal*, 59(2), 364–372. <https://doi.org/10.2136/sssaj1995.03615995005900020014x>
- Blake, G. R., & Hartge, K. H. (1986). Particle density. In A. Klute (Ed.), *Methods of soil analysis: Part 1. Physical and mineralogical methods* (pp. 377–382). SSSA and ASA.
- Caviezal, C., Hunziker, M., & Kuhn, N. (2017). Bequest of the Norseman—The potential for agricultural intensification and expansion in southern Greenland under climate change. *Land*, 6(4), 87. <https://doi.org/10.3390/land6040087>
- Chang, C.-W., Laird, D. A., Mausbach, M. J., & Hurburgh, C. R. (2001). Near-infrared reflectance spectroscopy—Principal components regression analyses of soil properties. *Soil Science Society of America Journal*, 65(2), 480–490. <https://doi.org/10.2136/sssaj2001.652480x>
- Christensen, J. H., Olesen, M., Boberg, F., Stendel, M., & Koldtoft, I. (2016). *Fremtidige klimaforandringer i Grønland: Kujalleq Kommune. Videnskabelig Rapport (15-04)*. Danish Meteorological Institute.
- Clark, R. N., King, T. V. V., Klejwa, M., Swayze, G. A., & Vergo, N. (1990). High spectral resolution reflectance spectroscopy of minerals. *Journal of Geophysical Research: Solid Earth*, 95(B8), 12653–12680. <https://doi.org/10.1029/JB095iB08p12653>
- Daanen, R. P., Ingeman-Nielsen, T., Marchenko, S. S., Romanovsky, V. E., Foged, N., Stendel, M., & Hornbech Svendsen, K. (2011). Permafrost degradation risk zone assessment using simulation models. *The Cryosphere*, 5(4), 1043–1056. <https://doi.org/10.5194/tc-5-1043-2011>
- Davari, M., Karimi, S. A., Bahrami, H. A., Taher Hossaini, S. M., & Fahmideh, S. (2021). Simultaneous prediction of several soil properties related to engineering uses based on laboratory Vis-NIR reflectance spectroscopy. *Catena*, 197, 104987. <https://doi.org/10.1016/j.catena.2020.104987>
- Deepagoda, T. K. K. C., Moldrup, P., Schjønning, P., Jonge, L. W. d., Kawamoto, K., & Komatsu, T. (2011). Density-corrected models for gas diffusivity and air permeability in unsaturated soil. *Vadose Zone Journal*, 10(1), 226–238. <https://doi.org/10.2136/vzj2009.0137>
- de Jong, S. (1993). SIMPLS: An alternative approach to partial least squares regression. *Chemometrics and Intelligent Laboratory Systems*, 18(3), 251–263. [https://doi.org/10.1016/0169-7439\(93\)85002-X](https://doi.org/10.1016/0169-7439(93)85002-X)
- Dexter, A. R., Richard, G., Arrouays, D., Czyż, E. A., Jolivet, C., & Duval, O. (2008). Complexed organic matter controls soil physical properties. *Geoderma*, 144(3), 620–627. <https://doi.org/10.1016/j.geoderma.2008.01.022>
- Dugmore, A. J., Keller, C., & McGovern, T. H. (2007). Norse Greenland settlement: Reflections on climate change, trade, and the contrasting fates of human settlements in the North Atlantic islands. *Arctic Anthropology*, 44(1), 12–36. <https://doi.org/10.1353/arc.2011.0038>
- Ernakovich, J. G., Wallenstein, M. D., & Calderón, F. J. (2015). Chemical indicators of cryoturbation and microbial processing throughout an Alaskan permafrost soil depth profile. *Soil Science Society of America Journal*, 79(3), 783–793. <https://doi.org/10.2136/sssaj2014.10.0420>
- Fang, Q., Hong, H., Zhao, L., Kukulich, S., Yin, K., & Wang, C. (2018). Visible and near-infrared reflectance spectroscopy for investigating soil mineralogy: A review. *Journal of Spectroscopy*, 2018, 3168974. <https://doi.org/10.1155/2018/3168974>
- Garde, A. A., Hamilton, M. A., Chadwick, B., Grocott, J., & McCaffrey, K. J. (2002). The Ketilidian orogen of South Greenland: Geochronology, tectonics, magmatism, and fore-arc accretion during Palaeoproterozoic oblique convergence. *Canadian Journal of Earth Sciences*, 39(5), 765–793. <https://doi.org/10.1139/e02-026>
- Gee, G. W., & Or, D. (2002). Particle-size analysis. In J. H. Dane & C. G. Topp (Eds.), *Methods of soil analysis: Part 4. Physical methods* (pp. 255–293). SSSA.
- Gowen, A. A., Downey, G., Esquerre, C., & O'Donnell, C. P. (2011). Preventing over-fitting in PLS calibration models of near-infrared (NIR) spectroscopy data using regression coefficients. *Journal of Chemometrics*, 25(7), 375–381. <https://doi.org/10.1002/cem.1349>
- Haaland, D. M., & Thomas, E. V. (1988). Partial least-squares methods for spectral analyses. 1. Relation to other quantitative calibration methods and the extraction of qualitative information. *Analytical Chemistry*, 60(11), 1193–1202. <https://doi.org/10.1021/ac00162a020>
- Hanna, E., & Cappelen, J. (2002). Recent climate of southern Greenland. *Weather*, 57(9), 320–328. <https://doi.org/10.1256/00431650260283497>
- Heiskanen, J. (1992). Comparison of three methods for determining the particle density of soil with liquid pycnometers. *Communications in Soil Science and Plant Analysis*, 23(7–8), 841–846. <https://doi.org/10.1080/00103629209368633>
- Hermansen, C., Knadel, M., Moldrup, P., Greve, M. H., Karup, D., & de Jonge, L. W. (2017). Complete soil texture is accurately predicted by visible near-infrared spectroscopy. *Soil Science Society of America Journal*, 81(4), 758–769. <https://doi.org/10.2136/sssaj2017.02.0066>
- Hoogsteen, M. J. J., Lantinga, E. A., Bakker, E. J., Groot, J. C. J., & Titttonell, P. A. (2015). Estimating soil organic carbon through loss on ignition: Effects of ignition conditions and structural water loss. *European Journal of Soil Science*, 66(2), 320–328. <https://doi.org/10.1111/ejss.12224>



- Hunt, G. R. (1977). Spectral signatures of particulate minerals in the visible and near infrared. *Geophysics*, 42(3), 501–513. <https://doi.org/10.1190/1.1440721>
- Islam, K., Singh, B., & McBratney, A. (2003). Simultaneous estimation of several soil properties by ultra-violet, visible, and near-infrared reflectance spectroscopy. *Soil Research*, 41(6), 1101–1114. <https://doi.org/10.1071/SR02137>
- Jensen, J. L., Christensen, B. T., Schjønning, P., Watts, C. W., & Munkholm, L. J. (2018). Converting loss-on-ignition to organic carbon content in arable topsoil: Pitfalls and proposed procedure. *European Journal of Soil Science*, 69(4), 604–612. <https://doi.org/10.1111/ejss.12558>
- Kögel-Knabner, I., & Amelung, W. (2021). Soil organic matter in major pedogenic soil groups. *Geoderma*, 384, 114785. <https://doi.org/10.1016/j.geoderma.2020.114785>
- Kokfelt, T. F., Weng, W. L., & Willerslev, E. (2019). *Geological map of South and South West Greenland - 1:100.000*. Geological Survey of Denmark and Greenland.
- Kuang, B., & Mouazen, A. M. (2011). Calibration of visible and near infrared spectroscopy for soil analysis at the field scale on three European farms. *European Journal of Soil Science*, 62(4), 629–636. <https://doi.org/10.1111/j.1365-2389.2011.01358.x>
- Manage, L. P. M., Katuwal, S., Norgaard, T., Knadel, M., Moldrup, P., de Jonge, L. W., & Greve, M. H. (2019). Estimating soil particle density using visible near-infrared spectroscopy and a simple, two-compartment pedotransfer function. *Soil Science Society of America Journal*, 83(1), 37–47. <https://doi.org/10.2136/sssaj2018.06.0217>
- McBride, R. A., Slessor, R. L., & Joosse, P. J. (2011). Estimating particle density from soil inventory data in the Lake Erie Lowlands. *Soil Survey Horizons*, 52(3), 94–98. <https://doi.org/10.2136/sh2011.3.0094>
- McBride, R. A., Slessor, R. L., & Joosse, P. J. (2012). Estimating the particle density of clay-rich soils with diverse mineralogy. *Soil Science Society of America Journal*, 76(2), 569–574. <https://doi.org/10.2136/sssaj2011.0177n>
- Moldrup, P., Olesen, T., Schjønning, P., Yamaguchi, T., & Rolston, D. E. (2000). Predicting the gas diffusion coefficient in undisturbed soil from soil water characteristics. *Soil Science Society of America Journal*, 64(1), 94–100. <https://doi.org/10.2136/sssaj2000.64194x>
- Mueller, C. W., Rethemeyer, J., Kao-Kniffin, J., Löppmann, S., Hinkel, K. M., & Bockheim, G. J. (2015). Large amounts of labile organic carbon in permafrost soils of northern Alaska. *Global Change Biology*, 21(7), 2804–2817. <https://doi.org/10.1111/gcb.12876>
- Norris, K. H. (2001). Understanding and correcting the factors which affect diffuse transmittance spectra. *NIR News*, 12(3), 6–9. <https://doi.org/10.1255/nirn.613>
- Nuttall, M. (2018). Arctic environments and peoples. In H. Callan (Ed.), *The international encyclopedia of anthropology* (pp. 1–7). John Wiley & Sons, Ltd.
- Ochsner, T. E., Horton, R., & Ren, T. (2001). A new perspective on soil thermal properties. *Soil Science Society of America Journal*, 65(6), 1641–1647. <https://doi.org/10.2136/sssaj2001.1641>
- Pribyl, D. W. (2010). A critical review of the conventional SOC to SOM conversion factor. *Geoderma*, 156(3), 75–83. <https://doi.org/10.1016/j.geoderma.2010.02.003>
- R Core Team. (2021). *R: A language and environment for statistical computing*. R Foundation for Statistical Computing.
- Redding, T. E., & Devito, K. J. (2006). Particle densities of wetland soils in northern Alberta, Canada. *Canadian Journal of Soil Science*, 86(1), 57–60. <https://doi.org/10.4141/s05-061>
- Redding, T. E., Hannam, K. D., Quideau, S. A., & Devito, K. J. (2005). Particle density of aspen, spruce, and pine forest floors in Alberta, Canada. *Soil Science Society of America Journal*, 69(5), 1503–1506. <https://doi.org/10.2136/sssaj2005.0018>
- Ruehlmann, J. (2020). Soil particle density as affected by soil texture and soil organic matter: 1. Partitioning of SOM in conceptual fractions and derivation of a variable SOC to SOM conversion factor. *Geoderma*, 375, 114542. <https://doi.org/10.1016/j.geoderma.2020.114542>
- Ruehlmann, J., & Körschens, M. (2020). Soil particle density as affected by soil texture and soil organic matter: 2. Predicting the effect of the mineral composition of particle-size fractions. *Geoderma*, 375, 114543. <https://doi.org/10.1016/j.geoderma.2020.114543>
- Rühlmann, J., Körschens, M., & Graefe, J. (2006). A new approach to calculate the particle density of soils considering properties of the soil organic matter and the mineral matrix. *Geoderma*, 130(3), 272–283. <https://doi.org/10.1016/j.geoderma.2005.01.024>
- Rutherford, G. K. (1995). Soils of some Norse settlements in south-western Greenland. *Arctic*, 48(4), 324–328. <https://doi.org/10.14430/arctic1254>
- Savitzky, A., & Golay, M. J. E. (1964). Smoothing and differentiation of data by simplified least squares procedures. *Analytical Chemistry*, 36(8), 1627–1639. <https://doi.org/10.1021/ac60214a047>
- Scheinost, A. C., Chavernas, A., Barrón, V., & Torrent, J. (1998). Use and limitations of second-derivative diffuse reflectance spectroscopy in the visible to near-infrared range to identify and quantify Fe oxide minerals in soils. *Clays and Clay Minerals*, 46(5), 528–536. <https://doi.org/10.1346/CCMN.1998.0460506>
- Schjønning, P., McBride, R. A., Keller, T., & Obour, P. B. (2017). Predicting soil particle density from clay and soil organic matter contents. *Geoderma*, 286, 83–87. <https://doi.org/10.1016/j.geoderma.2016.10.020>
- Serreze, M. C., & Barry, R. G. (2011). Processes and impacts of Arctic amplification: A research synthesis. *Global and Planetary Change*, 77(1), 85–96. <https://doi.org/10.1016/j.gloplacha.2011.03.004>
- Šimůnek, J., van Genuchten, M. T., & Šejna, M. (2008). Development and applications of the HYDRUS and STANMOD software packages and related codes. *Vadose Zone Journal*, 7(2), 587–600. <https://doi.org/10.2136/vzj2007.0077>
- Smith, D. M., Screen, J. A., Deser, C., Cohen, J., Fyfe, J. C., García-Serrano, J., & Zhang, X. (2019). The polar amplification model intercomparison project (PAMIP) contribution to CMIP6: Investigating the causes and consequences of polar amplification. *Geoscientific Model Development*, 12(3), 1139–1164. <https://doi.org/10.5194/gmd-12-1139-2019>
- Soane, B. D. (1990). The role of organic matter in soil compactibility: A review of some practical aspects. *Soil and Tillage Research*, 16(1), 179–201. [https://doi.org/10.1016/0167-1987\(90\)90029-D](https://doi.org/10.1016/0167-1987(90)90029-D)
- Stenberg, B., Viscarra Rossel, R. A., Mouazen, A. M., & Wetterlind, J. (2010). Visible and near infrared spectroscopy in soil science. *Advances in Agronomy*, 107, 163–215. [https://doi.org/10.1016/S0065-2113\(10\)07005-7](https://doi.org/10.1016/S0065-2113(10)07005-7)
- Sun, H., Nelson, M., Chen, F., & Husch, J. (2009). Soil mineral structural water loss during loss on ignition analyses. *Canadian Journal of Soil Science*, 89(5), 603–610. <https://doi.org/10.4141/CJSS09007>

- Upton, B. G. (2013). *Tectono-magmatic evolution of the younger Gardar southern rift, South Greenland* (GEUS Bulletin 29). Geological Survey of Denmark and Greenland. <https://doi.org/10.34194/geusb.v29.4692>
- Upton, B. G. J., Emeleus, C. H., Heaman, L. M., Goodenough, K. M., & Finch, A. A. (2003). Magmatism of the mid-Proterozoic Gardar Province, South Greenland: Chronology, petrogenesis and geological setting. *Lithos*, 68(1), 43–65. [https://doi.org/10.1016/S0024-4937\(03\)00030-6](https://doi.org/10.1016/S0024-4937(03)00030-6)
- Viscarra Rossel, R. A., & Behrens, T. (2010). Using data mining to model and interpret soil diffuse reflectance spectra. *Geoderma*, 158(1), 46–54. <https://doi.org/10.1016/j.geoderma.2009.12.025>
- Viscarra Rossel, R. A., McGlynn, R. N., & McBratney, A. B. (2006). Determining the composition of mineral-organic mixes using UV–vis–NIR diffuse reflectance spectroscopy. *Geoderma*, 137(1), 70–82. <https://doi.org/10.1016/j.geoderma.2006.07.004>
- Weber, P. L., de Jonge, L. W., Greve, M. H., Norgaard, T., & Moldrup, P. (2020). Gas diffusion characteristics of agricultural soils from South Greenland. *Soil Science Society of America Journal*, 84(5), 1606–1619. <https://doi.org/10.1002/saj2.20114>
- Weber, P. L., Hermansen, C., Norgaard, T., Pesch, C., Moldrup, P., Greve, M. H., & de Jonge, L. W. (2021). Moisture-dependent water repellency of Greenlandic cultivated soils. *Geoderma*, 402, 115189. <https://doi.org/10.1016/j.geoderma.2021.115189>
- Westergaard-Nielsen, A., Bjørnsson, A. B., Jepsen, M. R., Stendel, M., Hansen, B. U., & Elberling, B. (2015). Greenlandic sheep farming controlled by vegetation response today and at the end of the 21st Century. *Science of the Total Environment*, 512–513, 672–681. <https://doi.org/10.1016/j.scitotenv.2015.01.039>

## SUPPORTING INFORMATION

Additional supporting information can be found online in the Supporting Information section at the end of this article.

**How to cite this article:** Weber, P. L., Hermansen, C., Nørgaard, T., Pesch, C., Moldrup, P., Greve, M. H., Arthur, E., & de Jonge, L. (2022). Evaluating the particle densities of subarctic soils using pedotransfer functions and vis–NIR spectroscopy. *Soil Science Society of America Journal*, 86, 964–978. <https://doi.org/10.1002/saj2.20410>